

Stabilizing Cu⁺ in Cu/SiO₂ Catalysts with a Shattuckite-Like Structure Boosts CO₂ Hydrogenation into Methanol

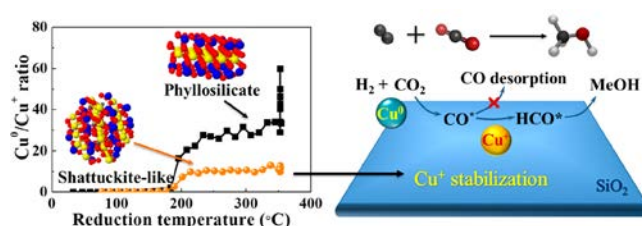
Jiafeng Yu,* Meng Yang, Jixin Zhang, Qingjie Ge, Anna Zimina,* Tim Pruessmann, Lei Zheng, Jan-Dierk Grunwaldt, and Jian Sun*

ABSTRACT: Cu based catalysts are widely employed for CO or CO₂ hydrogenation into methanol. However, their catalytic performance highly depends on supports, and the real evolution of Cu species is still covered by active components. Herein, we supply a Cu/SiO₂ catalyst prepared by flame spray pyrolysis (FSP), showing catalytic performance comparable to that of the active Cu/ZrO₂ catalyst for methanol synthesis from CO₂. It reaches 79% selectivity at a CO₂ conversion of 5.2%, which is an outstanding selectivity among previously reported Cu/SiO₂ catalysts, considering they are generally treated as nearly inert catalysts. *In situ* X ray absorption spectroscopy (XAS) analysis shows that 5 times more Cu⁺ species in the FSP Cu/SiO₂ are stabilized in comparison to those in the traditional ammonia evaporation (AE) made catalyst even after reduction at 350 °C. A unique shattuckite like precursor with a slightly distorted Cu–O–Si texture structure formed in the FSP made catalyst is responsible for the enriched Cu⁺ species. Variations of intermediate formation and methanol production are found to have a good relationship with the amount of Cu⁺ species. According to the results of high pressure *in situ* DRIFTS, we attribute this to the promotional effect of Cu⁺ on the stabilization of CO* intermediates, which inhibits CO desorption and facilitates further hydrogenation to CH₃OH via the RWGS + CO Hydro pathway. These results bring insights into the Cu reduction behavior and the function of Cu⁺ species during methanol production on Cu based catalysts without the assistance of active supports.

KEYWORDS: Cu/SiO₂ catalyst, CO₂ hydrogenation, methanol synthesis, synchrotron radiation, *in situ* X ray absorption spectroscopy

1. INTRODUCTION

In view of the severe CO₂ emission problem and its contribution to global warming, the production of methanol from CO₂ hydrogenation has been considered as a promising route for power to chemicals and CO₂ fixation, which has attracted extensive research recently.^{1–3} Methanol can be served as a platform intermediate for fuels and chemicals in the future due to its energy density and due to being easily storable and transportable, which is the basis of what is called the methanol economy.^{4–6} During methanol synthesis from CO₂, the main competitive process is the reverse water gas shift reaction (RWGS) to produce CO. An increase in CO₂ conversion has always been accompanied by a severe reduction in methanol selectivity due to thermodynamic equilibrium limitations.⁷ Considering the economic efficiency and practical applications, it is critical to develop highly efficient catalysts to enhance the methanol selectivity with an acceptable CO₂ conversion. However, most of the supported Cu based catalysts still suffer from low methanol selectivity at a passable CO₂ conversion (e.g., >10%). The methanol selectivity hardly exceeds 50% over traditional Cu Zn Al catalysts.^{8,9} Therefore, further developments of Cu based catalysts are promising in order to meet the requirements of high methanol selectivity at



low temperature for industrial applications, where methanol synthesis is more thermodynamically favorable.¹⁰

It has been reported that Cu⁰ as the active site could dissociate the adsorbed H₂, while Cu⁺ facilitates the conversion of intermediates by polarizing the C=O bond.^{11–13} The Cu⁺ species was supposed to be associated with CO₂ dissociation and also act as a stabilizer of the methoxy species,¹⁴ which could promote methanol synthesis. However, a linear relationship of the CO₂ conversion and CO production with the amount of Cu⁺ species was reported over Cu/SiO₂ catalysts at high temperature (260–380 °C),¹⁵ confirming the effect of Cu⁺ species on CO₂ activation and CO production. That leads to an inverse correlation of methanol selectivity with the fraction of Cu⁺ species. In addition, the function of Cu⁺ would be hidden if systems with active supports and dopants are investigated. Especially, “reducible” support oxides were

thought to be reactive components.¹⁶ For example, ZrO₂ was capable of stabilizing the intermediates¹⁷ and lowering the energy barrier pathway by facilitating formate intermediate formation and transformation.¹⁸ Methanol synthesis would be greatly enhanced via tuning Cu/Zr interactions,¹⁹ increasing oxygen vacancies,²⁰ and supplying basic sites.^{9,21} Moreover, it has been claimed for the dual site mechanism on Cu/ZnO that CO₂ adsorption and subsequent stepwise hydrogenation occurred on ZnO sites.^{22,23} An electron pair in the ZnO, Cu/Zn alloy and a less highly oxidized ZnO_x species were also reported to be active for methanol synthesis.^{24–26} Dynamic changes in Cu morphology were only observed in the Cu/ZnO system rather than in Cu/Al₂O₃ or Cu/SiO₂.²⁵ In view of this, the functions of Cu species and these active components are still not clear due to their complex interactions with each other. Furthermore, Cu⁰ was identified to be most of the active phase after a reduction pretreatment by XRD²⁷ and XAS,²⁸ while Cu⁺ was found to be the main component by XPS measurements.¹⁵ Some controversies still exist regarding the source of Cu⁺, the identification of Cu species in reduced samples, and the effect of Cu⁺ species on methanol selectivity. Therefore, it is better to evaluate the catalytic performance at low temperature (below 250 °C), where the methanol synthesis reaction dominates in the contributions to the CO₂ conversion rather than RWGS for Cu based catalysts. In addition, the identification of Cu⁺ species should be conducted via *in situ* techniques to avoid the overestimation of Cu⁺/Cu⁰ ratio by *ex situ* methods, because metallic Cu is easily oxidized in air. Finally, a detailed knowledge of the Cu valence state over a straightforward Cu catalyst with an inactive support for this reaction, e.g. Cu silicate, is desired, even though it may not be a good candidate for this reaction due to its poor performance.²⁹

In the present work, two Cu/SiO₂ catalysts with different Cu⁺ contents were successfully synthesized by ammonia evaporation (AE) and flame spray pyrolysis (FSP) methods via the formation of distinct types of Cu/Si precursors. FSP is a method of producing nanoparticles in an extremely short time (milliseconds) and at high temperature (2000 °C), which facilitates the formation of unique compounds. We provide a feasible strategy for stabilizing Cu⁺ species, an analysis of the Cu⁺ species stabilization mechanism, an observation of the reduction behavior of Cu oxides by *in situ* XAS, and a reaction pathway via *in situ* diffuse reflectance infrared Fourier transform spectroscopy (DRIFTS) at a real reaction pressure. The methanol selectivity of the Cu/SiO₂ catalyst made by FSP reaches a level that is comparable to that of the corresponding Cu/ZrO₂ catalyst, although the silica support without any dopants is thought to be inactive for the methanol synthesis. Thus, this work is expected to give a deep insight into the role of Cu⁺ species in enhancing methanol selectivity and to develop the potential function of “inert” supports.

2. EXPERIMENTAL SECTION

2.1. Catalyst Preparation. The FSP Cu/SiO₂ catalyst was prepared by the flame spray pyrolysis method as reported.^{30,31} Typically, the precursor solution was prepared by dissolving 1.5 g of cupric(II) acetylacetonate and 11.2 mL of tetraethyl orthosilicate (TEOS) in 100 mL of xylene at a final concentration of 0.5 M with reference to copper and silicon. The flame was generated by burning a mixture of CH₄ (0.6 L/min) and O₂ (1.9 L/min). The precursor was fed to the flame with a flow rate of 5 mL/min using a syringe pump (PHD UltraTM, Harvard) and dispersed by oxygen (feed rate 3.5 L/

min, pressure 1.5 bar). Nanoparticles were carried out of the flame by air with a feed rate of 5 L/min. The produced particles were collected on a water cooled glass fiber filter (Whatman GF/D, 25.7 cm in diameter) on the top of the cylinder with the help of a vacuum pump.

The AE Cu/SiO₂ catalyst was prepared by the conventional ammonia evaporation method as reported.²⁷ A 28% ammonia aqueous solution (Tianjin Kermel Corp.) was slowly added into a 0.3 M Cu(NO₃)₂·3H₂O (11.3 g, Tianjin Kermel Corp.) aqueous solution with agitation until the pH value remained constant at about 11. Afterward 12 g of SiO₂ nanoparticles (Evonik Degussa) was added to the obtained copper ammonia complex solution, and then the resulting solution continued to be stirred at 35 °C for 4 h. Ammonia evaporation was carried out by boiling the suspension at 90 °C until the pH value decreased to 6–7. The obtained sample was washed with deionized water and dried overnight at 120 °C. A calcination treatment was performed in the next step at 450 °C for 4 h in the air.

2.2. Catalyst Characterizations. The Cu loading was determined by inductively coupled plasma optical emission spectroscopy (PerkinElmer ICP OES 7300DV). The specific surface area was analyzed by nitrogen adsorption/desorption at 77 K using the BET method (Autosorb iQ2 by Quantachrome). Transmission electron microscopy (TEM) images were acquired using a JEOL JEM 2100 system with an acceleration voltage of 200 kV. The samples were prerduced at 350 °C for 0.5 h. X ray diffraction (XRD) data were collected on a PANalytical X'pert diffractometer equipped with a Cu K α source (running parameters: 40 kV, 40 mA). The Cu dispersion was measured by N₂O oxidation followed by the TPR method,³² which was carried out in a homemade setup.¹¹ After TPR under 5% H₂/95% Ar (30 mL/min), the sample was treated under a 5% N₂O/95% He (30 mL/min) atmosphere at 60 °C for 1 h to oxidize surface Cu atoms into Cu₂O. Then another TPR was performed again under the same conditions. The amount of H₂ consumed during the two processes was detected by TCD. The copper dispersion was calculated by dividing the amount of surface copper atoms by the total number of supported copper atoms per gram of the catalyst. The metallic copper surface area was computed on the basis of an atomic copper surface density of 1.46 × 10¹⁹ Cu atoms m⁻². CO TPD was performed on an automatic analyzer (Micromeritics Autochem 2910). The samples were first reduced under 10% H₂/90% Ar (30 mL/min) at 350 °C for 0.5 h and then purged by Ar (30 mL/min) at the same temperature for another 2 h. When the temperature was lowered to -50 °C with the help of liquid N₂, a 10% CO/90% He mixture gas flow was pulsed into the reactor at 4 min intervals. After adsorption saturation, the sample was purged with Ar until the baseline was stable. Then the furnace was heated to 800 °C with a temperature ramp of 10 °C/min. The desorbed CO was detected by TCD. The desorption peaks were fitted by the Gaussian–LorenCross method, and the R² values for AE Cu/SiO₂ and FSP Cu/SiO₂ catalysts were 0.99757 and 0.99869, respectively.

Fourier transform infrared (FTIR) spectra were recorded at room temperature on powdered samples in a Varian 3100 Fourier transform IR spectrometer. CO IR was conducted with a Bruker TENSOR 27 Fourier transform IR spectrometer. About 25 mg of the tabletted catalyst was put into the IR cell and then reduced at 350 °C (10 °C/min) for 0.5 h with a H₂ flow (99.99%) of 50 mL/min. After reduction, the sample was

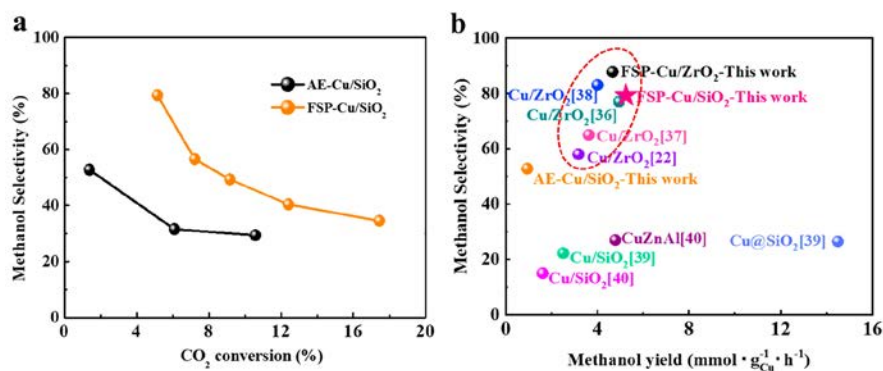


Figure 1. Catalytic performance of AE Cu/SiO₂ and FSP Cu/SiO₂ catalysts in the CO₂ hydrogenation reaction. (a) Selectivity–conversion relationships in CO₂ hydrogenation to methanol. Reaction conditions: 250 mg, 190–250 °C, 3.0 MPa, GHSV = 2040 h⁻¹. (b) Comparison of catalytic performance of Cu/SiO₂ catalysts in this work with other SiO₂ or ZrO₂ supported catalysts in the literature.^{21,36–40}

purged with N₂ (50 mL/min) at the same temperature for another 2 h, followed by cooling to room temperature. The background spectrum under this condition was recorded. Then, a 10% CO/90% He flow of 30 mL/min was introduced into the IR cell. After adsorption, a N₂ flow of 50 mL/min was used to purge the CO gas in the cell. During the adsorption and purging process, IR spectra were continuously recorded at 5 min intervals until the peak was unchanged. *In situ* diffuse reflectance infrared Fourier transform spectroscopy (*in situ* DRIFTS) at atmospheric pressure was performed on a Bruker VERTEX 70 Fourier transform IR spectrometer. The catalyst sample was first reduced in pure hydrogen (20 mL/min) at different temperatures, such as 200, 250, 300, and 350 °C for 10 min, and then purged with a 20 mL/min flow of He for 20 min at the same temperature. After each reduction process, the temperature was set to 230 °C, at which the background spectrum (200 scans) with a resolution of 4 cm⁻¹ was obtained. Subsequently, the spectra were recorded every 150 s in the Kubelka–Munk mode during the following procedure: (1) the sample was exposed to a 30% CO₂/70% He mixture (20 mL/min) and He (99.99%, 20 mL/min) gas flow at 230 °C for 30 min; (2) He (99.99%, 20 mL/min) was changed to H₂ (99.99%, 20 mL/min) and this flow was maintained for another 30 min; (3) the sample was purged with a 20 mL/min He flow for 30 min. Gas components in the outlet were monitored by a mass spectrometer. *In situ* DRIFTS at high pressure was performed by a similar procedure on a NICOLET 6700 Fourier transform IR spectrometer with PIKE Diffus IR device. The samples were first reduced at 300 °C for 0.5 h in pure H₂ and then swept and cooled to 230 °C under a He atmosphere. After a few minutes of stabilization, helium was changed into a CO₂ and H₂ mixture, and the pressure was increased to 3.0 MPa. The spectra (32 scans) with a resolution of 8 cm⁻¹ were continuously recorded during the reaction for 90 min.

In situ X ray photoelectron spectroscopy (XPS) with Auger electron spectroscopy (AES) was conducted with a Thermo Fischer ESCALAB 250Xi spectrometer. The X ray photoelectron spectra were obtained using Al K α radiation ($h\nu = 1486.6$ eV). The binding energies were calibrated by using the contaminant carbon (C 1s = 284.8 eV). First, XPS measurements of C 1s, O 1s, Cu 2p and Cu LM2 binding energies were conducted at room temperature for the as prepared catalysts. Then they were reduced *in situ* in pure H₂ (30 mL/min) at 300 °C for 0.5 h. Finally, the XPS measurement was repeated for the *in situ* reduced catalysts.

The X ray absorption spectroscopy (XAS) experiments were performed at the CAT ACT beamline at the Karlsruhe Institute of Technology (KIT) synchrotron facility.³³ The XAS data up to $k = 16$ Å⁻¹ at the Cu K (8979 eV) absorption edge were recorded at room temperature in transmission mode on the catalysts and reference materials (Cu metal foil and CuO and Cu₂O powders pressed into pellets). TPR was performed under a 5% H₂/95% He gas flow (50 mL/min) with a heating rate of 5 °C/min from room temperature up to 350 °C using a continuous flow capillary reactor (quartz, 1.5 mm outer diameter) filled with the catalysts (sieve fraction 100–200 μ m, 1:1 diluted with preformed SiO₂). The reduction process was continued at 350 °C for 0.5 h. During TPR, short Cu K spectra up to $k = 5$ Å⁻¹ were recorded (2.5 min per spectrum). Before and after the TPR the XAS data up to $k = 12$ Å⁻¹ at room temperature were recorded on samples in the capillary under an inert gas atmosphere. All of the data were processed and analyzed using the IFFEFIT software package.³⁴ The time resolved XAS spectrum was analyzed by linear combination analysis (LCA) with three standard spectra: Cu, Cu₂O and CuO. The *ex situ* X ray absorption data of the reduced AE Cu/SiO₂ sample at the Cu K absorption edge were recorded at room temperature in transmission mode at beamline BL14W1³⁵ of the Shanghai Synchrotron Radiation Facility (SSRF) in China.

2.3. Activity Tests. The catalytic performance of the catalysts was tested in a fixed bed stainless steel tubular reactor with a quartz liner with an inner diameter of 6 mm. Typically, 0.25 g of the sieved catalyst (sieve fraction of 425–850 μ m; bed length of 45 mm) was reduced at 350 °C under atmospheric pressure for 1 h in a pure hydrogen flow with a ramp rate of 1 °C/min before the reaction. The evaluation of catalytic performance was performed at 190–250 °C under a steady state (after 1 h on stream, Figure S1) under the conditions of 3.0 MPa and GHSV of 2040 h⁻¹ with a hydrogen/CO₂ (H/C) molar ratio of 3. All lines were heated to 150 °C to prevent the condensation of methanol and water. The products at the reactor outlet were detected with two online gas chromatographs (Shimadzu GC 8A and GC 14C) equipped with a thermal conductivity detector (TCD) and a flame ionization detector (FID), respectively. The TCD was used to analyze CO, CO₂ and N₂, where N₂ was used as an internal standard for volume correction. The FID was used for hydrocarbons, alcohols and other C containing products.

Conversion and selectivity in the catalytic tests were calculated as follows:

Table 1. Physicochemical Properties of the Cu/SiO₂ Samples

sample	Cu loading ^a (%)	D _{Cu} ^b (%)	S _{Cu} ^c (m ² /g)	d _{Cu} ^d (nm)	S _{BET} ^e (m ² /g)
AE-Cu/SiO ₂	17.0	37.8	41.4	2.6	350
FSP-Cu/SiO ₂	17.8	26.1	29.9	3.8	209

^aMeasured by ICP OES. ^bCu dispersion was determined by N₂O surface oxidation followed by TPR. ^cCu metal surface area based on an atomic surface density of 1.46 × 10¹⁹ Cu atoms m⁻². ^dCu metal particle size determined by the Cu dispersion. ^eSurface area of Cu/SiO₂ samples.

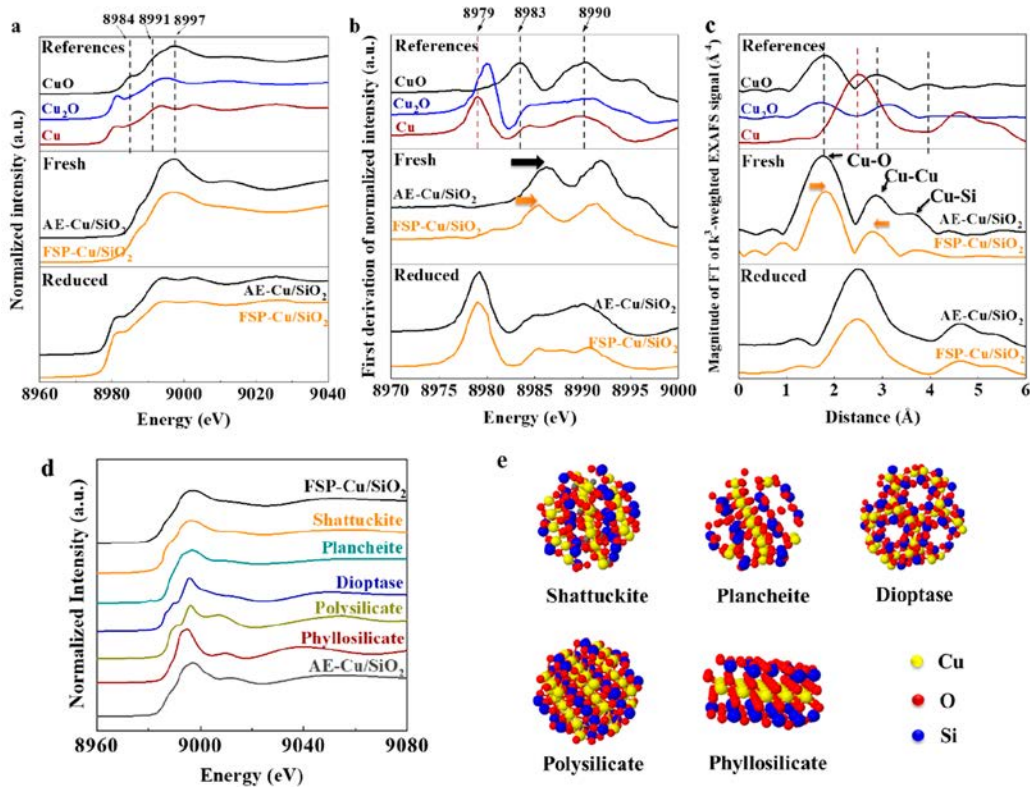


Figure 2. Structure analysis of Cu precursor: (a) Cu K XANES spectra, (b) the corresponding first derivatives of normalized spectra, and (c) Fourier transforms of k^3 weighted Cu K EXAFS signals of fresh and *in situ* reduced Cu/SiO₂ samples (350 °C for 0.5 h) as well as reference materials. (d) Comparison of XAS Cu K spectra of AE and FSP samples with those of theoretically calculated reference structures. (e) Crystal structure models of shattuckite, plancheite, diopside, polysilicate, and phyllosilicate Cu–Si compounds.

$$\text{conversion: } X(\text{CO}_2) = \left(1 - \frac{\text{CO}_{2,\text{out}} \times N_{2,\text{in}}}{N_{2,\text{out}} \times \text{CO}_{2,\text{in}}} \right) \times 100\%$$

yield:

$$Y(\text{CH}_3\text{OH}) = \frac{\text{CH}_3\text{OH}_{\text{out}}}{\text{CH}_3\text{OH}_{\text{out}} + \text{CO}_{\text{out}} + \text{CO}_2_{\text{out}}} \times 100\%$$

$$\text{selectivity: } S(\text{CH}_3\text{OH}) = \frac{Y(\text{CH}_3\text{OH})}{X(\text{CO}_2)} \times 100\%$$

3. RESULTS AND DISCUSSION

3.1. Catalytic Performance. Generally, the selectivity to methanol decreases with increasing temperature, which is due to a higher contribution of the endothermic RWGS reaction.⁴¹ As expected, a negative correlation was noticed between methanol selectivity and CO₂ conversion on both investigated catalysts, as shown in Figure 1a. The Cu/SiO₂ catalyst made by ammonia evaporation (AE) was chosen here because it is usually believed to be the most effective preparation method with highly dispersed Cu nanoparticles for Cu/SiO₂ catalysts,

usually exhibiting higher methanol selectivity in comparison with impregnated catalysts in the literature. In comparison, the FSP Cu/SiO₂ catalyst shows both higher CO₂ conversion and higher methanol selectivity, even better than those of AE Cu/SiO₂, which is a breakthrough for a Cu/SiO₂ catalyst without any active components. For the former, the methanol selectivity can reach 79.3%, which is extremely high in comparison to 31.5% for the latter when they perform the same CO₂ conversion at about 5%. Under the same conditions, the methanol yield of FSP Cu/SiO₂ is almost 0.9 mmol g_{cat}⁻¹ h⁻¹ at extremely low temperature (190 °C), which is 5.6 times more than that of AE Cu/SiO₂ (see Figure S2). The turnover frequency (TOF) of methanol synthesis is 1.2 h⁻¹ for the former, while it is 0.16 h⁻¹ for the latter. Actually, as shown in Figure 1b (details in Table S1), the conventional Cu/SiO₂ series catalysts without any dopants or promoters were not good candidates for methanol synthesis from CO₂ due to their low methanol selectivity,²⁹ which was caused by the lack of formate species formation.¹⁸ ZrO₂ supported Cu catalysts have been widely accepted to have a better catalytic performance in comparison to SiO₂ supported Cu catalysts⁴¹ as shown in the marked area of Figure 1b due to the capability of facilitating

the conversion of adsorbed CO₂ to formate intermediates and further transformation into formaldehyde or methoxy at the Cu/ZrO₂ interface.⁴² Moreover, it has been reported that the methanol selectivity can be enhanced to the corresponding Cu/ZrO₂ level as long as only small amounts of isolated Zr(IV) surface sites exist on SiO₂ support.²⁹ Also, similar surface intermediates (formate and methoxy) can be observed over the modified Cu/SiO₂ with isolated surface Zr(IV), while these are never seen on Cu/SiO₂ catalysts.²⁹ The industrial CuZnAl catalysts exhibit high activity but always suffer from low methanol selectivity. To the best of our knowledge, a high methanol selectivity has never been obtained on Cu/SiO₂ without any other active phases. Herein, a significantly enhanced catalytic performance, especially the methanol selectivity, was achieved over the FSP Cu/SiO₂ catalyst without any dopants, reaching a high level comparable to those of Cu/ZrO₂ catalysts both in the literatures and the catalyst made in house. Therefore, a detailed knowledge of Cu species over the simple Cu catalyst with an inactive support (Cu/SiO₂) and their catalytic mechanism via *in situ* characterizations is required, even though it may be not the best candidate for this reaction. Any promotion obtained from the Cu/SiO₂ catalyst is meaningful to better understand the real Cu function without the effects of the other active components, which would benefit the further development of Cu based catalysts.

3.2. Characterizations of Catalyst Structure. The physicochemical properties of the fresh Cu/SiO₂ samples made by FSP and AE are given in Table 1. The surface area of fresh AE Cu/SiO₂ is much higher than that of the FSP sample due to the formation of a layered copper phyllosilicate precursor, as proven by the appearance of the $\delta(\text{OH})$ vibration at 670 cm⁻¹ and the $\nu(\text{SiO})$ shoulder peak at 1040 cm⁻¹ in FTIR measurements^{11,43} (see Figure S3). In the FSP sample, the band at 670 cm⁻¹ is absent, and the band at 1040 cm⁻¹ is strongly reduced, both revealing that the precursor is distinct from copper phyllosilicate. From the results of surface oxidation of reduced samples by N₂O followed by TPR, the Cu particle sizes of AE and FSP samples were both estimated to be around 3 nm. This coincides with the TEM results (images given in Figure S4). The coexistence of Cu and Cu₂O was observed from *ex situ* XRD patterns (Figure S5) in both the reduced and used samples. These results show that the Cu particle sizes and dispersions of the two samples are similar. The distinct performances were probably caused by different Cu species. It is worth noting that the identification of Cu species, including Cu⁰ and Cu⁺, in these samples demands more convincing proof executed by *in situ* studies, since the reduced copper particles are very sensitive to air.⁴⁴

Copper species on the fresh and *in situ* reduced samples (350 °C for 0.5 h) were studied by Cu K X ray absorption near edge structure (XANES) spectroscopy via comparison with the data obtained from the reference materials (Figure 2a). The spectra of both fresh samples resemble that of the bulk CuO, but the shape and the position of characteristic absorption edge features are significantly different. The most pronounced difference is the shift of the low energy shoulders, which is attributed to a 1s–4p transition to Cu 4p–O 2s π orbitals of octahedrally coordinated Cu²⁺ compounds (in CuO at 8984 eV) and the transitions corresponding to σ orbitals (in CuO at 8991 eV),⁴⁵ by about 2.5 and 1.5 eV to higher energies in AE and FSP catalysts, respectively. This difference becomes more obvious when the first derivatives of the corresponding XANES

spectra are compared (Figure 2b). These changes hint at a different ligand charge transfer due to an altered Cu local geometric structure in the Cu–O–Si precursor in comparison to CuO.^{28,46,47}

The phase corrected Fourier transforms of k^3 weighted Cu K extended X ray absorption fine structure (EXAFS) signals of all the samples before and after *in situ* reduction are shown in Figure 2c. For both fresh samples, the shapes of the Fourier transformed scattering resemble that of bulk CuO up to high order shells with some differences in the position and intensity of the backscattering peaks. The main backscattering peak around 1.8 Å corresponds to a Cu–O shell in CuO, while the smaller peak around 2.9 Å corresponds to a Cu–Cu shell in CuO (C1₂/c1 space group, $a = 4.6837$ Å, $b = 3.4226$ Å, $c = 5.128$ Å, $\alpha = 90^\circ$, $\beta = 99.54^\circ$, $\gamma = 90^\circ$). In the fresh FSP sample, the Cu–O peak is slightly shifted to a greater distance and the Cu–Cu peak is shifted to a lower distance, indicating a stronger distortion of the CuO₆ octahedra in comparison to the AE sample. The peak at longer distances might be related to the scattering on the higher coordination shells containing Si, O and Cu. In case of highly crystalline silicate, one would expect a Cu–Si peak to be visible above 3 Å, exhibiting the arrangement of the silicon ions around the Cu ion.

The coordination numbers (CNs) from EXAFS fitting (Table S2) in both Cu–O and Cu–Cu shells are lower in the fresh FSP sample in comparison to the AE sample, hinting at an increase in the disorder around the Cu site. The distortion can probably be attributed to the changes in the crystal field around the Cu octahedral (O_h) site due to the bonding to the SiO₄ blocks, where the presence of an Si ion causes changes in the local charge on the connecting oxygen ions. Such metastable oxides with local structure distortion between metal and oxygen atoms are also observed in other FSP materials,⁴⁸ which may result from the quenching process from extremely high temperature during the preparation process. Moreover, the low CNs, which do not match well with the particle size observed in TEM, may be attributed to the distortion of Cu–O–Si compounds with different Cu–O distances.

The spectroscopic data for the fresh sample are compared in Figure 2d to the theoretical simulations of the Cu K XANES spectra based on the standard structures of different copper silicates and their crystal models using the FMDNES program⁴⁹ and to the available experimental data on copper silicates.⁵⁰ Combining the XRD, IR, N₂ physisorption, and XANES results and theoretical considerations, we propose that a copper phyllosilicate with a layered structure (Figure 2e) is formed in the AE sample, while a more packed structure Cu–O–Si compound similar to shattuckite (Figure 2e), where short islands of CuO_x are placed between the SiO₄ blocks, is formed in the FSP sample (Figure S6). The Cu²⁺ ion in shattuckite is situated in an elongated octahedron,⁵¹ and the CuO₆ octahedron has a strong tetragonal distortion,⁵² so that the spectroscopic results are in agreement with these findings. In addition, other related structures could be at the origin of the observed altered structure.

After the *in situ* reduction, most of the Cu species in both samples were reduced into metallic Cu (see XANES data in Figure 2a,b and EXAFS data in Figure 2c). The EXAFS data of both reduced AE and FSP samples are identical with those obtained for metallic Cu, including the higher shells, indicating the formation of well ordered metallic Cu particles. Note that we also collected the *ex situ* XAS spectra of the reduced AE

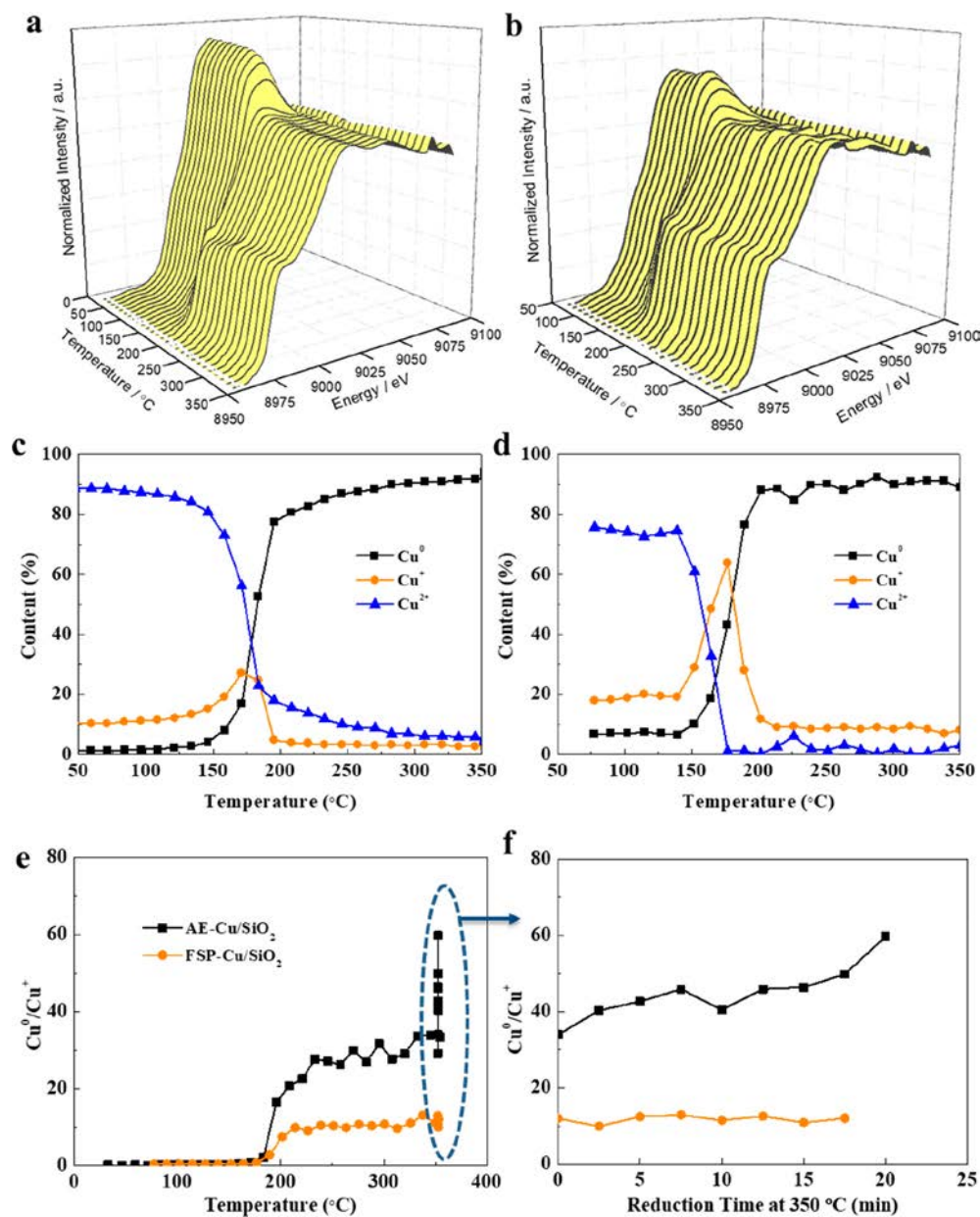


Figure 3. Normalized Cu K edge XANES spectra during TPR of (a) AE Cu/SiO₂ and (b) FSP Cu/SiO₂ from room temperature to 350 °C. The contents of the chemical state of Cu species (Cu⁰, Cu⁺ and Cu²⁺) of (c) AE Cu/SiO₂ and (d) FSP Cu/SiO₂ during the TPR experiment. (e) Variations of Cu⁰/Cu⁺ ratio over AE Cu/SiO₂ and FSP Cu/SiO₂ samples during TPR experiments. (f) Cu⁰/Cu⁺ ratio versus reduction time at 350 °C.

sample, where Cu⁺ species appeared and became the dominant ones (Figure S7). The discrepancy in the results show that reduced metallic Cu is easily oxidized on exposure to air. To clarify the state of the naturally oxidized Cu/SiO₂, the reduced FSP sample was further oxidized at 300 °C for 0.5 h under a flow of synthetic air. The XAS spectra collected during the reduction–oxidation process are shown in Figure S8. After reduction, large numbers of Cu⁰ species are formed. During the following oxidation treatment, they neither completely reverse back to the initial structure of Cu precursor nor can be oxidized into CuO. The shape of the XANES spectrum at a low energy site is slightly different from those of both the fresh FSP sample and the CuO reference, indicating the interaction between Cu and Si also has an effect on the oxidation of Cu. The Cu precursor in the fresh FSP sample contains unique

species distinguished from CuO, which coincides with the above analysis.

3.3. Identification of Reduction Behavior. *In situ* XANES measurements were performed during the TPR to monitor the changes in the oxidation state and local structure of copper species during reduction. As shown in Figure 3a,b, the white line feature of Cu²⁺ gradually decreases, while the pre edge feature at 8981 eV assigned to Cu⁰ gradually appears with an increase in temperature for both studied samples.

The distribution of Cu⁰, Cu⁺ and Cu²⁺ for AE Cu/SiO₂ and FSP Cu/SiO₂ samples during TPR was calculated on the basis of a linear combination analysis (LCA) using the first derivatives of the reference compounds corrected for the experimentally observed energy shifts and plotted in Figure 3c,d, respectively. Detailed comparisons of each Cu species can

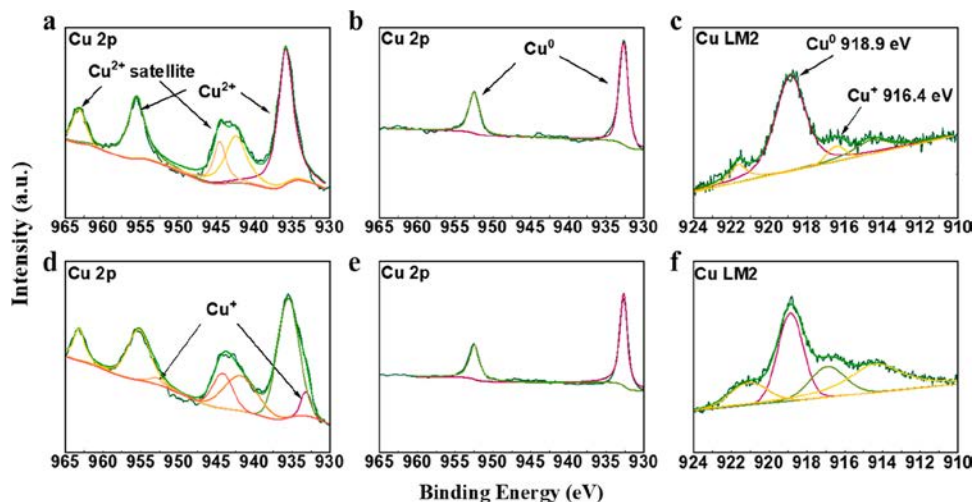


Figure 4. *In situ* XPS AES spectra of AE Cu/SiO₂ (a–c) and FSP Cu/SiO₂ (d–f), where (a) and (d) are Cu 2p of as prepared catalysts, (b) and (e) are Cu 2p of reduced catalysts, and (c) and (f) are Cu LM2 of reduced catalysts.

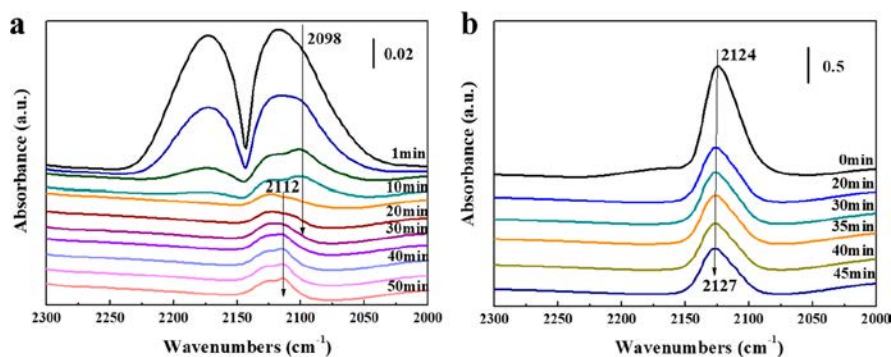


Figure 5. Variations of IR spectra during N₂ purging treatments at 20 °C of (a) AE Cu/SiO₂ and (b) FSP Cu/SiO₂ samples after CO adsorption. The samples were reduced *in situ* at 350 °C for 0.5 h before CO adsorption.

be found in Figures S9 and S10. In the AE Cu/SiO₂ sample, the reduction was step by step from Cu²⁺ to Cu⁺ (step I) and then from Cu⁺ to Cu⁰ (step II). These two steps started at about 150 °C. At first, the reduction rate of step II was slower than that of step I, leading to the accumulation of Cu⁺ species to 27%. Afterward, the rate of step II exceeded that of step I with increasing temperature. In this process, the amount of Cu⁰ sharply increased, accompanied by a decrease in Cu²⁺ and Cu⁺ until 200 °C. The reduction behavior of the FSP Cu/SiO₂ sample was distinctly different. The reduction of Cu²⁺ started at a temperature close to 150 °C and was quickly completed at 170 °C. At this point, pronounced Cu⁺ species accumulation was observed with a maximum of 64%, as a result of a much slower rate for step II in comparison to step I. Furthermore, in contrast to the AE sample, a still significant amount of Cu⁺ can be found in the reduced FSP sample even at a high temperature of 350 °C, perhaps resulting from the texture structure of Cu–Si compounds where Cu species are incorporated in a silica matrix and thus stabilized.^{47,53}

The Cu⁰/Cu⁺ ratios for both samples are plotted in Figure 3e as a function of temperature and of reduction time. The ratio in FSP Cu/SiO₂ remained stable at around 11 even at 350 °C. In contrast, it gradually increased to 33 in AE Cu/SiO₂ at 350 °C and further increased to 60 when the same temperature was maintained for 20 min (Figure 3f). This high extent of reduction of the copper phyllosilicate precursor was also found via *in situ* XRD results in our previous work.²⁷ In

FSP Cu/SiO₂, about 8.3% of the Cu⁺ species cannot be reduced even at 350 °C over long times, which is about 5 times more than that in AE sample (1.6%) under the same conditions. This stabilization function of Cu⁺ species were also found in FSP Cu/TiO₂ catalysts.⁵⁴

In situ XPS AES was performed here to further quantify the Cu⁺/Cu⁰ ratio, as shown in Figure 4. Four Cu 2p peaks for Cu²⁺ and its satellite were clearly observed for both as prepared samples. A small amount of Cu⁺ species was detected on FSP Cu/SiO₂ in Figure 4d but not on AE Cu/SiO₂ in Figure 4a. After *in situ* reduction treatment, CuO species were completely reduced. Cu LM2 from AES was measured to further identify Cu⁰ and Cu⁺ species. As shown in Figure 4c,f, a binding energy of 918.9 eV was ascribed to Cu⁰ species, while that at 916.4 eV was assigned to Cu⁺ species. The Cu⁺/(Cu⁰ + Cu⁺) ratios were identified to be 7.5 and 33.6% for AE and FSP Cu/SiO₂, respectively. Although a slightly higher absolute value was obtained in comparison to XAS results due to different fitting methods of these two techniques, the tendency of Cu⁺ contents from AES remained consistent with XAS fitting, demonstrating that XAS fitting was an efficient method to evaluate the valence state of Cu. Moreover, the variations of Cu states were able to be monitored during the reduction process for XAS rather than the AES technique.

3.4. Chemical Adsorption Performance. Fourier transform infrared (FT IR) spectroscopy is commonly applied to probe the chemical state and distribution of Cu species on the

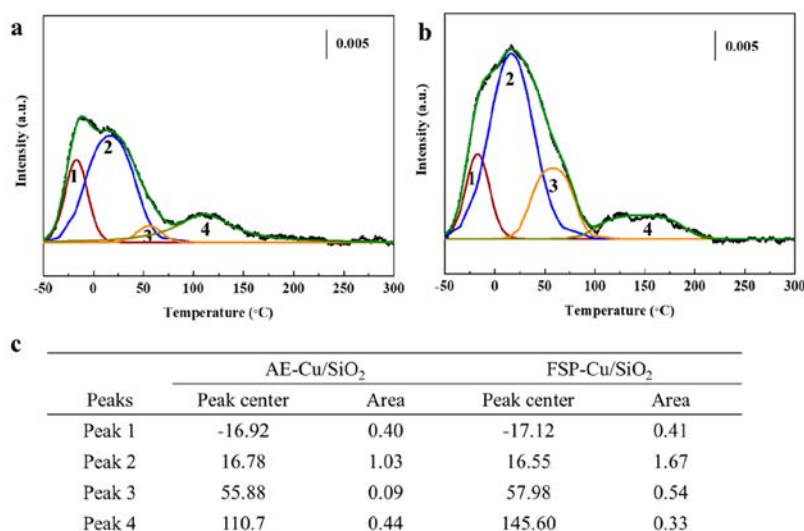


Figure 6. CO TPD results of (a) AE Cu/SiO₂ and (b) FSP Cu/SiO₂ samples with peak fitting list (c), where the unit of the peak centers is °C.

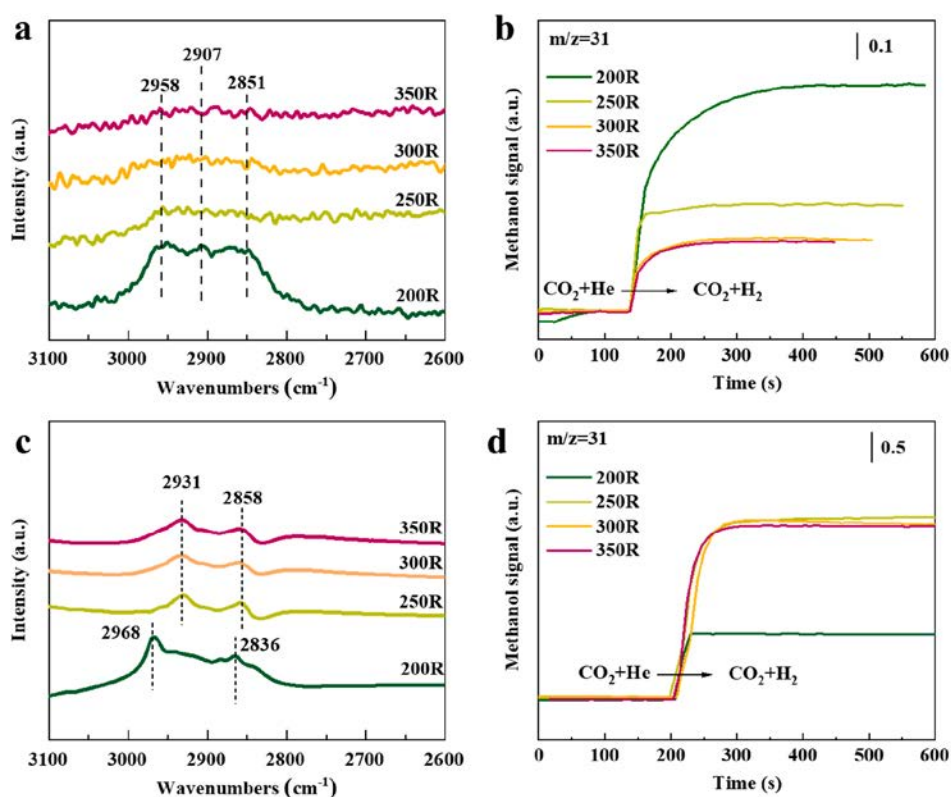


Figure 7. *In situ* DRIFTS spectra of the CO₂ hydrogenation after CO₂ absorption on (a, b) AE Cu/SiO₂ and (c, d) FSP Cu/SiO₂ catalysts after reduction at different temperatures, where (b) and (d) give the methanol signal (m/z 31) from a mass spectrometer after the IR reactor, respectively, during the atmosphere switch from CO₂ + He to CO₂ + H₂. Reaction conditions: 30% CO₂/70% He, 99.99% He and 99.99% H₂ all at a flow rate of 20 mL/min, 0.1 MPa, 230 °C.

catalyst surface after CO adsorption. The IR spectra were collected on the reduced AE and FSP Cu/SiO₂ catalysts (350 °C for 0.5 h) during CO adsorption (see Figure S11), where physisorption and chemisorption coexisted on the catalyst surface. During N₂ purging, the physisorbed CO gradually disappeared. Two chemisorbed CO bands for both the AE and FSP samples remained (see Figure 5a,b, respectively). According to peak fitting in Figure S12, bands at 2127 and 2112 cm⁻¹ with a ratio of 0.8 for the AE sample can be

assigned to linear stretching of Cu⁺-CO and Cu⁰-CO species, respectively,^{55,56} while the ratio increased to 1.8 for the FSP sample.

Additionally, CO TPD was executed to quantify the amount of CO adsorption on different Cu species from -50 °C due to its weak adsorption at room temperature. Four desorption peaks can be found for each reduced sample in Figure 6a,b. In comparison to the blank experiment of the SiO₂ support, peak 4 belongs to CO adsorbed on SiO₂ (Figure S13). CO

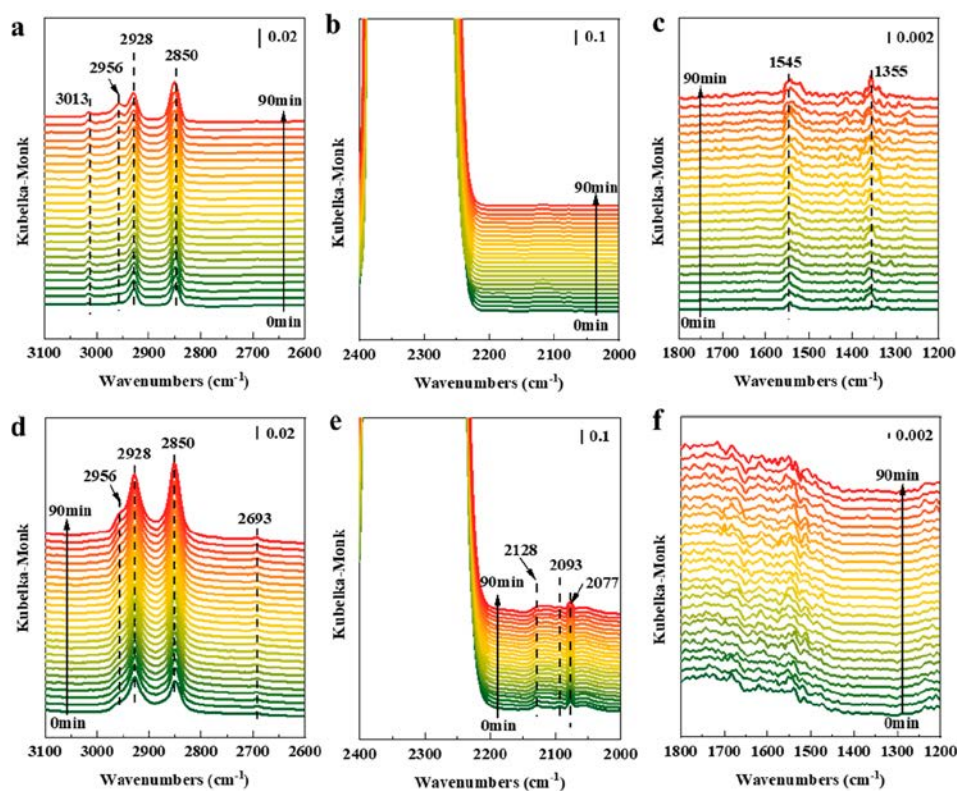


Figure 8. *In situ* DRIFTS spectra of (a–c) AE Cu/SiO₂ and (d–f) FSP Cu/SiO₂ during the CO₂ + H₂ reaction at high pressure. Reduction conditions: 300 °C for 30 min in a pure H₂ flow (20 mL/min). Reaction conditions: CO₂/H₂ = 1/3, 3.0 MPa, 230 °C.

adsorption on Cu species can be divided into two parts. The first part represents weakly adsorbed CO including peaks 1 and 2, which will not appear in FT IR spectra, since CO desorbs below room temperature. The second part can be assigned to the CO strongly adsorbed on Cu species (peak 3), which corresponds to the peaks observed in FT IR spectra. We suppose that most of the Cu⁰–CO species will desorb at room temperature, and the peak with a center at around 56 °C might be ascribed to Cu⁺–CO. According to peak area fitting in Figure 6c, the desorption peak area of Cu⁺–CO of the FSP sample is about 6 times larger than that of the AE sample, which coincides well with the XAS and XPS AES results.

3.5. Catalytic Mechanistic Analysis. *In situ* DRIFTS experiments were executed to investigate the relationship between intermediate formation and methanol production with Cu⁺ species via regulation of reduction temperatures. Although the inferred absorption peaks for Cu/SiO₂ catalysts are very weak at low pressure (0.1 MPa), three bands at 2958, 2907 and 2851 cm⁻¹ can be observed in Figure 7a for the low temperature (200 °C) reduced AE Cu/SiO₂ catalyst. With an increase in reduction temperature, the amount of Cu⁺ species decreases (see Figure S10); meanwhile, the coverage of intermediates decreases. Accordingly, the methanol production in the outlet detected via the mass spectrum (MS) in Figure 7b decreases with the reduction of Cu⁺ species. For low temperature reduced FSP Cu/SiO₂ (200R), the bands at 2968, 2887, 2866, 2836, 1566 and 1551 cm⁻¹ which belong to formate species obviously increase, while those at 2929 and 2857 cm⁻¹ assigned to methoxy species^{17,57} decrease with reaction time (Figure S14), indicating that the formate pathway is dominant after reduction at 200 °C. In comparison, with an increase in reduction temperature, the intermediates

formed on FSP Cu/SiO₂ change into methoxy species and remain constant, as observed in Figure 7c, which is consistent with unchanged Cu⁺ species as observed in Figure 3. The dominant pathway also changes from formate to RWGS + CO Hydro after reduction at higher temperature (above 250 °C). The methanol production measured by MS in Figure 7d is low at 200R but markedly increases and remains stable after reduction at 250 °C. Note that the real temperature at the catalyst surface which is very close to the window might be slightly lower than the temperature measured inside the DRIFTS cell. Thus, the specific phenomenon at 200R is probably caused by the unstable state during the transformation of different Cu species at around 180 °C (see Figure 3d). Nevertheless, a clear relationship between Cu⁺ species and methanol is observed, which demonstrates that the formation of Cu⁺ species is responsible for the enhancement of intermediate formation and methanol production.

Currently, the mechanism of CO₂ hydrogenation into methanol is still controversial among three main pathways: the formate pathway,⁵⁸ the RWGS + CO Hydro pathway,⁵⁹ and the hydrocarboxyl pathway.⁶⁰ Investigations on these routes reveal that the stabilization of key reaction intermediates is crucial for controlling catalytic selectivity. Here, *in situ* DRIFTS measurements were performed to identify the possible intermediates and pathways at a real reaction pressure (3.0 MPa) over Cu/SiO₂ catalysts, as shown in Figure 8. For both of the tested catalysts, two combination bands of CO₂ were observed at 3500–3800 cm⁻¹ (Figure S15)⁶¹ and three main peaks were detected in the region of 2600–3100 cm⁻¹. The bonds at 2850 and 2928 cm⁻¹ are assigned to the symmetric and asymmetric H₂CO* stretching vibrations, respectively,^{62,63} which may derive from both formate and

RWGS + CO Hydro pathways. The band at 2928 cm^{-1} can be also attributed to the $\nu(\text{CH}_3)$ modes of the H_3CO^* species.¹⁷ The feature at 2956 cm^{-1} is a combination of the CH bending and asymmetric OCO stretching modes of bidentate formate species.¹⁷ The intensities of all three peaks increase with reaction time to some extent, as shown in Figure S16. In detail, the intensity ratio of the band at 2956 cm^{-1} compared to that at 2850 cm^{-1} , which represents the proportion of the formate pathway, slightly decreases from 33.3 to 31.3% for the FSP Cu/SiO₂ catalyst after a 90 min reaction, while it obviously increases from 13.2 to 38.5% for AE Cu/SiO₂ under the same conditions. This reveals that the CO* hydrogenation to H₂CO* could remain stable over FSP Cu/SiO₂ due to the inhibition of CO desorption and stabilization of CO* species. Moreover, small bands at 1545 and 1355 cm^{-1} , which are assigned to asymmetric and symmetric OCO stretching vibrations, respectively, of adsorbed bidentate HCOO* species, are only detected for AE Cu/SiO₂. Meanwhile, the band at 2693 cm^{-1} assigned to asymmetric $-\text{CH}_2$ stretching of *H₂CO species⁶⁴ as well as the features at 2077 , 2093 and 2128 cm^{-1} belonging to CO* adsorption⁶⁵ on both Cu⁰ and Cu⁺ sites⁶⁶ can only be observed for FSP Cu/SiO₂.

On the basis of the comprehensive results of *in situ* XAS, *in situ* DRIFTS, FTIR and TPD, the formation of a unique catalyst structure and a modified reaction mechanism for the FSP Cu/SiO₂ catalyst are proposed in Figure S17 and Figure 9,

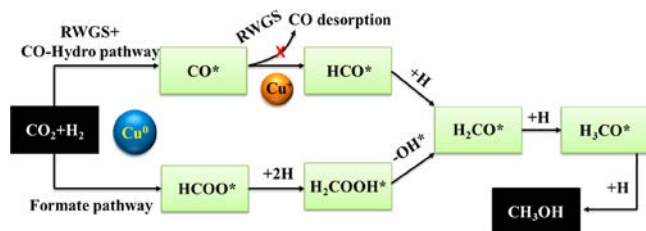


Figure 9. Reaction scheme for CO₂ hydrogenation to CH₃OH at Cu⁰ and Cu⁺ active sites via the RWGS + CO Hydro and Formate pathways. Asterisks indicate adsorbed species.

respectively. The nanoparticles containing Cu and Si components were created at extremely high temperature in the flame and quickly carried up by a large high speed air flow. The as prepared catalysts were collected by the filter on the top without further calcination. The collected Cu/SiO₂ catalysts contained CuO nanoparticles and shattuckite like species with strongly interacting Cu–Si entities and a disordered Cu–O–Si texture structure; these are finally reduced into Cu⁰ and Cu⁺ species in the process of prereluction treatment, respectively. The FSP method could supply both CuO and shattuckite materials at the same time with highly dispersed Cu nanoparticles, which made this method more promising in comparison to the direct use of shattuckite materials.

As shown in Figure 9, the formate and RWGS + CO Hydro pathways both exist during the CO₂ hydrogenation process. Strong signals of a methoxy intermediate and some formate species were observed from *in situ* DRIFTS spectra for both catalysts. However, for the RWGS + CO Hydro pathway, CO bonding should be moderate, being strong enough to prevent desorption but weak enough to allow further hydrogenation to HCO*.¹⁷ Therefore, the key point in inhibiting CO desorption and enhancing further hydrogenation is to stabilize the CO*

intermediate. CO TPD results showed that CO adsorption was stronger on Cu⁺ than on Cu⁰ species, which facilitates further hydrogenation to occur on Cu⁺ over FSP Cu/SiO₂ due to the inhibition of CO desorption and the stabilization of CO* species. The selectivity to CH₃OH is enhanced over FSP Cu/SiO₂ due to the promoted stability of the CO* intermediates, which enables the CO* hydrogenation to CH₃OH to be more competitive with CO desorption in the RWGS + CO Hydro pathway. In addition, Cu⁺ species such as a suboxidic Cu_xO structure below the Cu surface might be responsible for CO₂ adsorption and activation.⁶⁷ Meanwhile, Cu⁰ species are the active sites for H₂ activation, which are essential for the first hydrogenation step in both the formate and RWGS + CO Hydro pathways. Therefore, Cu⁰ should be the main component in catalysts to maintain high CO₂ conversion, and with this prerequisite, Cu⁺ helps to increase the methanol selectivity.

4. CONCLUSION

Reduction behaviors of the Cu/SiO₂ catalysts made by AE and FSP preparation methods have been intensively investigated via an *in situ* XAS technique, focusing on the analysis of the local structure of Cu species and their changes with respect to the valence state during the reduction process. About 8.3% of the Cu⁺ species remain stable in the SiO₂ matrix even after reduction at 350 °C for the FSP sample, which is about 5 times more than that in the AE sample. The observed particular reduction behavior of Cu species is related to a distorted Cu–O–Si structure, similar to that in shattuckite, which stabilizes Cu⁺ species, and therefore might be a key option to regulate the distribution of various Cu species via formation of distinct precursors. The variations of Cu⁺ species are consistent with intermediate formation during the reaction as well as methanol production via regulating reduction temperatures. Moreover, the high pressure *in situ* DRIFTS results show that Cu⁺ species could help to inhibit CO desorption and further facilitate CO* hydrogenation to CH₃OH by stabilizing CO* intermediates, promoting the RWGS + CO Hydro pathway. Thus, the stabilization of 5 times more Cu⁺ species on FSP Cu/SiO₂ in comparison to the AE catalyst is responsible for the significant enhancement of methanol selectivity from 31.5 to 79.3% when they perform the same CO₂ conversion at about 5%, which reaches a catalytic performance comparable to that of Cu/ZrO₂. The recognition of the Cu oxide reduction behavior and the role of Cu⁺ species in this work shed light on the understanding of the catalytic mechanism of methanol synthesis from CO₂. We also supplied here a feasible strategy to improve catalytic performance by controlling the structure of the Cu species.

AUTHOR INFORMATION

Corresponding Authors

Jiafeng Yu – Dalian Institute of Chemical Physics, Chinese Academy of Sciences, Dalian 116023, People's Republic of China; Institute of Catalysis Research and Technology,

Karlsruhe Institute of Technology, 76344 Eggenstein Leopoldshafen, Germany; orcid.org/0000 0003 4314 1324; Email: yujf@dicp.ac.cn

Anna Zimina – Institute of Catalysis Research and Technology, Karlsruhe Institute of Technology, 76344 Eggenstein Leopoldshafen, Germany; Institute for Chemical Technology and Polymer Chemistry, Karlsruhe Institute of Technology, 76131 Karlsruhe, Germany; orcid.org/0000 0002 3111 7741; Email: anna.zimina@kit.edu

Jian Sun – Dalian Institute of Chemical Physics, Chinese Academy of Sciences, Dalian 116023, People's Republic of China; orcid.org/0000 0002 4191 578X; Email: sunj@dicp.ac.cn

Authors

Meng Yang – Dalian Institute of Chemical Physics, Chinese Academy of Sciences, Dalian 116023, People's Republic of China; University of Chinese Academy of Sciences, Beijing 100049, People's Republic of China

Jixin Zhang – Dalian Institute of Chemical Physics, Chinese Academy of Sciences, Dalian 116023, People's Republic of China

Qingjie Ge – Dalian Institute of Chemical Physics, Chinese Academy of Sciences, Dalian 116023, People's Republic of China; orcid.org/0000 0003 3345 014X

Tim Pruessmann – Institute of Nuclear Waste Disposal, Karlsruhe Institute of Technology, 76344 Eggenstein Leopoldshafen, Germany; orcid.org/0000 0002 7903 9199

Lei Zheng – Institute for Chemical Technology and Polymer Chemistry, Karlsruhe Institute of Technology, 76131 Karlsruhe, Germany

Jan Dierk Grunwaldt – Institute of Catalysis Research and Technology, Karlsruhe Institute of Technology, 76344 Eggenstein Leopoldshafen, Germany; Institute for Chemical Technology and Polymer Chemistry, Karlsruhe Institute of Technology, 76131 Karlsruhe, Germany; orcid.org/0000 0003 3606 0956

Complete contact information is available at: <https://pubs.acs.org/10.1021/acscatal.0c04371>

Author Contributions

J.Y. proposed the conception of this work, conducted the preparation and characterization of the catalysts, analyzed the data, and wrote the manuscript. M.Y. tested the catalytic performance. J.Z. helped with the preparation experiments. A.Z. and T.P. performed the XAS characterizations and calculations. L.Z. participated in the DRIFTS characterization. Q.G. and J.D.G. helped in the discussion and revised the manuscript. J.S. was in charge of the project, contributed the interpretation of data, and revised the manuscript.

Notes

The authors declare no competing financial interest.

ACKNOWLEDGMENTS

This study was supported by the DICP (Grant DICP I202012), the Natural Science Foundation of China (Grant 21403215), the Liaoning Revitalization Talents Program (XLYC1907066), and the Youth Innovation Promotion Association of Chinese Academy of Sciences (2018214). The authors thank the Institute for Beam Physics and Technology (IBPT/KIT) for the operation at the storage ring in the

Karlsruhe Research Accelerator (KARA), beamline BL14W1 (Shanghai Synchrotron Radiation Facility) for providing the beamtime, and the NS TEST Co. (<http://www.ns.catalysis.com>) for the high pressure *in situ* DRIFTS measurements.

REFERENCES

- (1) Álvarez, A.; Bansode, A.; Urakawa, A.; Bavykina, A. V.; Wezendonk, T. A.; Makkee, M.; Gascon, J.; Kapteijn, F. Challenges in the Greener Production of Formates/Formic Acid, Methanol, and DME by Heterogeneously Catalyzed CO₂ Hydrogenation Processes. *Chem. Rev.* **2017**, *117* (14), 9804–9838.
- (2) Kalz, K. F.; Kraehnert, R.; Dvoyashkin, M.; Dittmeyer, R.; Gläser, R.; Krewer, U.; Reuter, K.; Grunwaldt, J. D. Future Challenges in Heterogeneous Catalysis: Understanding Catalysts under Dynamic Reaction Conditions. *ChemCatChem* **2017**, *9*, 17–29.
- (3) Schlögl, R. E. Mobility and the Energy Transition. *Angew. Chem., Int. Ed.* **2017**, *56* (37), 11019–11022.
- (4) Olah, G. A. Beyond Oil and Gas: The Methanol Economy. *Angew. Chem., Int. Ed.* **2005**, *44* (18), 2636–2639.
- (5) Bukhtiyarova, M.; Lunkenbein, T.; Kähler, K.; Schlögl, R. Methanol Synthesis from Industrial CO₂ Sources: A Contribution to Chemical Energy Conversion. *Catal. Lett.* **2017**, *147* (2), 416–427.
- (6) Behrens, M.; Studt, F.; Kasatkin, I.; Kühl, S.; Hävecker, M.; Abild Pedersen, F.; Zander, S.; Girgsdies, F.; Kurr, P.; Knief, B. L.; Tovar, M.; Fischer, R. W.; Nørskov, J. K.; Schlögl, R. The Active Site of Methanol Synthesis over Cu/ZnO/Al₂O₃ Industrial Catalysts. *Science* **2012**, *336* (6083), 893–897.
- (7) Gaikwad, R.; Bansode, A.; Urakawa, A. High pressure advantages in stoichiometric hydrogenation of carbon dioxide to methanol. *J. Catal.* **2016**, *343*, 127–132.
- (8) Zhang, L.; Zhang, Y.; Chen, S. Effect of promoter SiO₂, TiO₂ or SiO₂ TiO₂ on the performance of CuO ZnO Al₂O₃ catalyst for methanol synthesis from CO₂ hydrogenation. *Appl. Catal., A* **2012**, *415–416*, 118–123.
- (9) Gao, P.; Li, F.; Zhao, N.; Xiao, F.; Wei, W.; Zhong, L.; Sun, Y. Influence of modifier (Mn, La, Ce, Zr and Y) on the performance of Cu/Zn/Al catalysts via hydrotalcite like precursors for CO₂ hydrogenation to methanol. *Appl. Catal., A* **2013**, *468*, 442–452.
- (10) Jiang, X.; Nie, X.; Guo, X.; Song, C.; Chen, J. G. Recent Advances in Carbon Dioxide Hydrogenation to Methanol via Heterogeneous Catalysis. *Chem. Rev.* **2020**, *120*, 7984.
- (11) Gong, J.; Yue, H.; Zhao, Y.; Zhao, S.; Zhao, L.; Lv, J.; Wang, S.; Ma, X. Synthesis of Ethanol via Syngas on Cu/SiO₂ Catalysts with Balanced Cu⁰–Cu⁺ Sites. *J. Am. Chem. Soc.* **2012**, *134* (34), 13922–13925.
- (12) Sun, J.; Yu, J.; Ma, Q.; Meng, F.; Wei, X.; Sun, Y.; Tsubaki, N. Freezing copper as a noble metal-like catalyst for preliminary hydrogenation. *Sci. Adv.* **2018**, *4* (12), eaau3275.
- (13) Li, F.; Wang, L.; Han, X.; He, P.; Cao, Y.; Li, H. Influence of support on the performance of copper catalysts for the effective hydrogenation of ethylene carbonate to synthesize ethylene glycol and methanol. *RSC Adv.* **2016**, *6* (51), 45894–45906.
- (14) Chen, C. S.; Cheng, W. H.; Lin, S. S. Mechanism of CO formation in reverse water–gas shift reaction over Cu/Al₂O₃ catalyst. *Catal. Lett.* **2000**, *68* (1), 45–48.
- (15) Wang, Z. Q.; Xu, Z. N.; Peng, S. Y.; Zhang, M. J.; Lu, G.; Chen, Q. S.; Chen, Y.; Guo, G. C. High Performance and Long Lived Cu/SiO₂ Nanocatalyst for CO₂ Hydrogenation. *ACS Catal.* **2015**, *5* (7), 4255–4259.
- (16) Behrens, M. Heterogeneous Catalysis of CO₂ Conversion to Methanol on Copper Surfaces. *Angew. Chem., Int. Ed.* **2014**, *53* (45), 12022–12024.
- (17) Kattel, S.; Yan, B.; Yang, Y.; Chen, J. G.; Liu, P. Optimizing Binding Energies of Key Intermediates for CO₂ Hydrogenation to Methanol over Oxide Supported Copper. *J. Am. Chem. Soc.* **2016**, *138* (38), 12440–12450.

- (18) Fisher, I. A.; Bell, A. T. In Situ Infrared Study of Methanol Synthesis from H₂/CO over Cu/SiO₂ and Cu/ZrO₂/SiO₂. *J. Catal.* **1998**, *178* (1), 153–173.
- (19) Tada, S.; Kayamori, S.; Honma, T.; Kamei, H.; Nariyuki, A.; Kon, K.; Toyao, T.; Shimizu, K. i.; Satokawa, S. Design of Interfacial Sites between Cu and Amorphous ZrO₂ Dedicated to CO₂ to Methanol Hydrogenation. *ACS Catal.* **2018**, *8* (9), 7809–7819.
- (20) Samson, K.; Śliwa, M.; Socha, R. P.; Góra Marek, K.; Mucha, D.; Rutkowska Zbik, D.; Paul, J. F.; Ruggiero Mikolajczyk, M.; Grabowski, R.; Sloczyński, J. Influence of ZrO₂ Structure and Copper Electronic State on Activity of Cu/ZrO₂ Catalysts in Methanol Synthesis from CO₂. *ACS Catal.* **2014**, *4* (10), 3730–3741.
- (21) Guo, X.; Mao, D.; Lu, G.; Wang, S.; Wu, G. The influence of La doping on the catalytic behavior of Cu/ZrO₂ for methanol synthesis from CO₂ hydrogenation. *J. Mol. Catal. A: Chem.* **2011**, *345* (1), 60–68.
- (22) Le Valant, A.; Comminges, C.; Tisseraud, C.; Canaff, C.; Pinard, L.; Pouilloux, Y. The Cu–ZnO synergy in methanol synthesis from CO₂, Part I: Origin of active site explained by experimental studies and a sphere contact quantification model on Cu+ZnO mechanical mixtures. *J. Catal.* **2015**, *324*, 41–49.
- (23) Kanai, Y.; Watanabe, T.; Fujitani, T.; Saito, M.; Nakamura, J.; Uchijima, T. Evidence for the migration of ZnO_x in a Cu/ZnO methanol synthesis catalyst. *Catal. Lett.* **1994**, *27* (1), 67–78.
- (24) Brown, N. J.; Weiner, J.; Hellgardt, K.; Shaffer, M. S. P.; Williams, C. K. Phosphinate stabilised ZnO and Cu colloidal nanocatalysts for CO₂ hydrogenation to methanol. *Chem. Commun.* **2013**, *49* (94), 11074–11076.
- (25) Grunwaldt, J. D.; Molenbroek, A. M.; Topsøe, N. Y.; Topsøe, H.; Clausen, B. S. In Situ Investigations of Structural Changes in Cu/ZnO Catalysts. *J. Catal.* **2000**, *194* (2), 452–460.
- (26) Schott, V.; Oberhofer, H.; Birkner, A.; Xu, M.; Wang, Y.; Muhler, M.; Reuter, K.; Wöll, C. Chemical Activity of Thin Oxide Layers: Strong Interactions with the Support Yield a New Thin Film Phase of ZnO. *Angew. Chem., Int. Ed.* **2013**, *52* (45), 11925–11929.
- (27) Dong, X.; Ma, X.; Xu, H.; Ge, Q. Comparative study of silica supported copper catalysts prepared by different methods: formation and transition of copper phyllosilicate. *Catal. Sci. Technol.* **2016**, *6* (12), 4151–4158.
- (28) Grandjean, D.; Pelipenko, V.; Batyrev, E. D.; Heuvel, J. C. V. D.; Khassin, A. A.; Yurieva, T. M.; Weckhuysen, B. M. Dynamic Cu/Zn Interaction in SiO₂ Supported Methanol Synthesis Catalysts Unraveled by in Situ XAFS. *J. Phys. Chem. C* **2011**, *115* (41), 20175–20191.
- (29) Lam, E.; Larmier, K.; Wolf, P.; Tada, S.; Safonova, O. V.; Copéret, C. Isolated Zr Surface Sites on Silica Promote Hydrogenation of CO₂ to CH₃OH in Supported Cu Catalysts. *J. Am. Chem. Soc.* **2018**, *140* (33), 10530–10535.
- (30) Yu, J.; Zhang, Z.; Dallmann, F.; Zhang, J.; Miao, D.; Xu, H.; Goldbach, A.; Dittmeyer, R. Facile synthesis of highly active Rh/Al₂O₃ steam reforming catalysts with preformed support by flame spray pyrolysis. *Appl. Catal., B* **2016**, *198*, 171–179.
- (31) Mueller, R.; Mädler, L.; Pratsinis, S. E. Nanoparticle synthesis at high production rates by flame spray pyrolysis. *Chem. Eng. Sci.* **2003**, *58* (10), 1969–1976.
- (32) Van Der Grift, C. J. G.; Wielers, A. F. H.; Jogh, B. P. J.; Van Beunum, J.; De Boer, M.; Versluijs Helder, M.; Geus, J. W. Effect of the reduction treatment on the structure and reactivity of silica supported copper particles. *J. Catal.* **1991**, *131* (1), 178–189.
- (33) Zimina, A.; Dardenne, K.; Denecke, M. A.; Doronkin, D. E.; Huttel, E.; Lichtenberg, H.; Mangold, S.; Pruessmann, T.; Rothe, J.; Spangenberg, T.; Steininger, R.; Vitova, T.; Geckeis, H.; Grunwaldt, J. D. CAT ACT—A new highly versatile x ray spectroscopy beamline for catalysis and radionuclide science at the KIT synchrotron light facility ANKA. *Rev. Sci. Instrum.* **2017**, *88* (11), 113113.
- (34) Ravel, B.; Neville, M. ATHENA, ARTEMIS, HEPHAESTUS: data analysis for X ray absorption spectroscopy using IFEFFIT. *J. Synchrotron Radiat.* **2005**, *12* (4), 537–541.
- (35) Haisheng, Y.; Xiangjun, W.; Jiong, L.; Songqi, G.; Shuo, Z.; Zheng, J.; Yuying, H. The XAFS beamline of SSRF. *Nucl. Sci. Technol.* **2015**, *05*, 6–12.
- (36) Kilo, M.; Weigel, J.; Wokaun, A.; Koepfel, R. A.; Stoeckli, A.; Baiker, A. Effect of the addition of chromium and manganese oxides on structural and catalytic properties of copper/zirconia catalysts for the synthesis of methanol from carbon dioxide. *J. Mol. Catal. A: Chem.* **1997**, *126* (2), 169–184.
- (37) Shi, Z.; Tan, Q.; Wu, D. Ternary copper cerium zirconium mixed metal oxide catalyst for direct CO₂ hydrogenation to methanol. *Mater. Chem. Phys.* **2018**, *219*, 263–272.
- (38) Arena, F.; Italiano, G.; Barbera, K.; Bordiga, S.; Bonura, G.; Spadaro, L.; Frusteri, F. Solid state interactions, adsorption sites and functionality of Cu ZnO/ZrO₂ catalysts in the CO₂ hydrogenation to CH₃OH. *Appl. Catal., A* **2008**, *350* (1), 16–23.
- (39) Yang, H.; Gao, P.; Zhang, C.; Zhong, L.; Li, X.; Wang, S.; Wang, H.; Wei, W.; Sun, Y. Core-shell structured Cu@m SiO₂ and Cu/ZnO@m SiO₂ catalysts for methanol synthesis from CO₂ hydrogenation. *Catal. Commun.* **2016**, *84*, 56–60.
- (40) Jiang, X.; Koizumi, N.; Guo, X.; Song, C. Bimetallic Pd–Cu catalysts for selective CO₂ hydrogenation to methanol. *Appl. Catal., B* **2015**, *170–171*, 173–185.
- (41) Li, K.; Chen, J. G. CO₂ Hydrogenation to Methanol over ZrO₂ Containing Catalysts: Insights into ZrO₂ Induced Synergy. *ACS Catal.* **2019**, *9* (9), 7840–7861.
- (42) Ihm, S. K.; Park, Y. K.; Jeon, J. K.; Park, K. C.; Lee, D. K.; Inui, T.; Anpo, M.; Izui, K.; Yanagida, S.; Yamaguchi, T. A study on methanol synthesis through CO₂ hydrogenation over copper based catalysts. *Stud. Surf. Sci. Catal.* **1998**, *114*, 505–508.
- (43) Song, Y.; Zhang, J.; Lv, J.; Zhao, Y.; Ma, X. Hydrogenation of Dimethyl Oxalate over Copper Based Catalysts: Acid–Base Properties and Reaction Paths. *Ind. Eng. Chem. Res.* **2015**, *54* (40), 9699–9707.
- (44) Ma, X.; Yang, Z.; Liu, X.; Tan, X.; Ge, Q. Dynamic redox cycle of Cu⁰ and Cu⁺ over Cu/SiO₂ catalyst in ester hydrogenation. *RSC Adv.* **2015**, *5* (47), 37581–37584.
- (45) DuBois, J. L.; Mukherjee, P.; Stack, T. D. P.; Hedman, B.; Solomon, E. I.; Hodgson, K. O. A Systematic K edge X ray Absorption Spectroscopic Study of Cu(III) Sites. *J. Am. Chem. Soc.* **2000**, *122* (24), 5775–5787.
- (46) Lytle, F. W.; Greegor, R. B.; Panson, A. J. Discussion of x ray absorption near edge structure: Application to Cu in the high T_c superconductors La_{1.8}Sr_{0.2}CuO₄ and YBa₂Cu₃O₇. *Phys. Rev. B: Condens. Matter Mater. Phys.* **1988**, *37* (4), 1550–1562.
- (47) Kappen, P.; Grunwaldt, J. D.; Hammershoi, B. S.; Tröger, L.; Clausen, B. S. The State of Cu Promoter Atoms in High Temperature Shift Catalysts An in Situ Fluorescence XAFS Study. *J. Catal.* **2001**, *198* (1), 56–65.
- (48) Zhang, Z.; Yu, J.; Zhang, J.; Ge, Q.; Xu, H.; Dallmann, F.; Dittmeyer, R.; Sun, J. Tailored metastable Ce Zr oxides with highly distorted lattice oxygen for accelerating redox cycles. *Chem. Sci.* **2018**, *9* (13), 3386–3394.
- (49) Bunaű, O.; Joly, Y. Self consistent aspects of x ray absorption calculations. *J. Phys.: Condens. Matter* **2009**, *21* (21), 345501.
- (50) Farges, F.; Benzerara, K.; Brown, G. E. Chrysocolla Redefined as Spertiniite. *AIP Conf. Proc.* **2006**, *882* (1), 223–225.
- (51) Sarma, K. B. N.; Reddy, B. J.; Lakshman, S. V. J. Absorption spectra of Cu²⁺ in shattuckite and plancheite. *Phys. Lett. A* **1982**, *92* (6), 305–308.
- (52) Feng, W. L. Theoretical explanation of absorption spectra and ESR parameters of Cu²⁺ in shattuckite. *Phys. B* **2012**, *407* (18), 3865–3867.
- (53) Yamaguchi, A.; Shido, T.; Inada, Y.; Kogure, T.; Asakura, K.; Nomura, M.; Iwasawa, Y. Time resolved DXAFS study on the reduction processes of Cu cations in ZSM 5. *Catal. Lett.* **2000**, *68* (3), 139–145.
- (54) Yang, F.; Liu, M.; Chen, X.; Xu, Z.; Zhao, H. Simultaneous Control over Lattice Doping and Nanocluster Modification of a

Hybrid CuO_x/TiO₂ Photocatalyst during Flame Synthesis for Enhancing Hydrogen Evolution. *Solar RRL* **2018**, *2* (12), 1800215.

(55) Hadjiivanov, K.; Knözinger, H. FTIR study of CO and NO adsorption and coadsorption on a Cu/SiO₂ catalyst: Probing the oxidation state of copper. *Phys. Chem. Chem. Phys.* **2001**, *3* (6), 1132–1137.

(56) Di, W.; Cheng, J.; Tian, S.; Li, J.; Chen, J.; Sun, Q. Synthesis and characterization of supported copper phyllosilicate catalysts for acetic ester hydrogenation to ethanol. *Appl. Catal., A* **2016**, *510*, 244–259.

(57) Wang, Y.; Kattel, S.; Gao, W.; Li, K.; Liu, P.; Chen, J. G.; Wang, H. Exploring the ternary interactions in Cu–ZnO–ZrO₂ catalysts for efficient CO₂ hydrogenation to methanol. *Nat. Commun.* **2019**, *10* (1), 1166.

(58) Larmier, K.; Liao, W. C.; Tada, S.; Lam, E.; Verel, R.; Bansode, A.; Urakawa, A.; Comas Vives, A.; Copéret, C. CO₂ to Methanol Hydrogenation on Zirconia Supported Copper Nanoparticles: Reaction Intermediates and the Role of the Metal–Support Interface. *Angew. Chem., Int. Ed.* **2017**, *56* (9), 2318–2323.

(59) Tang, Q. L.; Hong, Q. J.; Liu, Z. P. CO₂ fixation into methanol at Cu/ZrO₂ interface from first principles kinetic Monte Carlo. *J. Catal.* **2009**, *263* (1), 114–122.

(60) Gao, L. Z.; Au, C. T. CO₂ Hydrogenation to Methanol on a YBa₂Cu₃O₇ Catalyst. *J. Catal.* **2000**, *189* (1), 1–15.

(61) Fehr, S. M.; Krossing, I. Spectroscopic Signatures of Pressurized Carbon Dioxide in Diffuse Reflectance Infrared Spectroscopy of Heterogeneous Catalysts. *ChemCatChem* **2020**, *12* (9), 2622–2629.

(62) Lu, R.; Gan, W.; Wu, B. h.; Chen, H.; Wang, H. f. Vibrational Polarization Spectroscopy of CH Stretching Modes of the Methylene Group at the Vapor/Liquid Interfaces with Sum Frequency Generation. *J. Phys. Chem. B* **2004**, *108* (22), 7297–7306.

(63) Smidt, E.; Eckhardt, K. U.; Lechner, P.; Schulten, H. R.; Leinweber, P. Characterization of different decomposition stages of biowaste using FT IR spectroscopy and pyrolysis field ionization mass spectrometry. *Biodegradation* **2005**, *16* (1), 67–79.

(64) Ratna, D.; Divekar, S.; Samui, A. B.; Chakraborty, B. C.; Banthia, A. K. Poly(ethylene oxide)/clay nanocomposite: Thermo mechanical properties and morphology. *Polymer* **2006**, *47* (11), 4068–4074.

(65) Schumann, J.; Kröhnert, J.; Frei, E.; Schlögl, R.; Trunschke, A. IR Spectroscopic Study on the Interface of Cu Based Methanol Synthesis Catalysts: Evidence for the Formation of a ZnO Overlayer. *Top. Catal.* **2017**, *60* (19), 1735–1743.

(66) Bailey, S.; Froment, G. F.; Snoeck, J. W.; Waugh, K. C. A DRIFTS study of the morphology and surface adsorbate composition of an operating methanol synthesis catalyst. *Catal. Lett.* **1995**, *30* (1), 99–111.

(67) Favaro, M.; Xiao, H.; Cheng, T.; Goddard, W. A.; Yano, J.; Crumlin, E. J. Subsurface oxide plays a critical role in CO₂ activation by Cu(111) surfaces to form chemisorbed CO₂, the first step in reduction of CO₂. *Proc. Natl. Acad. Sci. U. S. A.* **2017**, *114* (26), 6706–6711.

Repository KITopen

Dies ist ein Postprint/begutachtetes Manuskript.

Empfohlene Zitierung:

Yu, J.; Yang, M.; Zhang, J.; Ge, Q.; Zimina, A.; Pruessmann, T.; Zheng, L.; Grunwaldt, J.-D.; Sun, J.

[Stabilizing Cu⁺ in Cu/SiO₂ Catalysts with a Shattuckite-Like Structure Boosts CO₂ Hydrogenation into Methanol](#)

2020. ACS catalysis, 10

[doi: 10.554/IR/1000127799](#)

Zitierung der Originalveröffentlichung:

Yu, J.; Yang, M.; Zhang, J.; Ge, Q.; Zimina, A.; Pruessmann, T.; Zheng, L.; Grunwaldt, J.-D.; Sun, J.

[Stabilizing Cu⁺ in Cu/SiO₂ Catalysts with a Shattuckite-Like Structure Boosts CO₂ Hydrogenation into Methanol](#)

2020. ACS catalysis, 10 (24), 14694–14706.

[doi:10.1021/acscatal.0c04371](#)

Lizenzinformationen: [KITopen-Lizenz](#)